

Accepted Article Preview: Published ahead of advance online publication



Photosensitive Material Enabling Direct Fabrication of Filigree 3D Silver Microstructures via Laser-Induced Photoreduction

Erik Hagen Waller, Julian Karst and Georg von Freymann

Cite this article as: Erik Hagen Waller, Julian Karst and Georg von Freymann. Photosensitive Material Enabling Direct Fabrication of Filigree 3D Silver Microstructures via Laser-Induced Photoreduction. *Light: Advanced Manufacturing*. accepted article preview 9 February 2021; doi: 10.37188/lam.2021.008

This is a PDF file of an unedited peer-reviewed manuscript that has been accepted for publication. LAM are providing this early version of the manuscript as a service to our customers. The manuscript will undergo copyediting, typesetting and a proof review before it is published in its final form. Please note that during the production process errors may be discovered which could affect the content, and all legal disclaimers apply.

Received 13 July 2020; revised 2 February 2021; accepted 8 February 2021;
Accepted article preview online 9 February 2021

1 Photosensitive Material Enabling Direct Fabrication of Filigree 3D Silver 2 Microstructures via Laser-Induced Photoreduction

3
4 Erik Hagen Waller^{1,2}, Julian Karst³ and Georg von Freymann^{1,2}

5
6 [1] Fraunhofer Institute for industrial mathematics ITWM, 67663 Kaiserslautern, Germany

7 E-mail: erik.waller@itwm.fraunhofer.de, georg.von.freymann@itwm.fraunhofer.de

8 [2] Physics Department and Research Center OPTIMAS, Technische Universität

9 Kaiserslautern, 67663 Kaiserslautern, Germany

10 [3] 4th Physics Institute and Research Center SCoPE, University of Stuttgart, 70569 Stuttgart,
11 Germany

12 Corresponding author:

13 Erik Hagen Waller (erik.waller@itwm.fraunhofer.de)

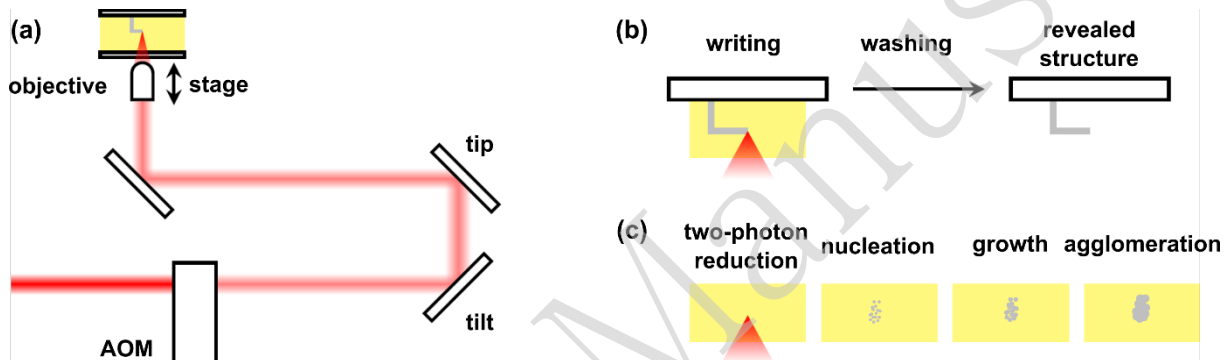
14
15
16 **Keywords:** 3D printing, microelectronics, on-chip fabrication

17 Introductory Paragraph

18 Laser-induced photoreduction (LPR) as a direct fabrication technique that promises to be one
19 of the most versatile routes for fabricating highly conductive 3D metallic microstructures on-
20 chip (e.g., metamaterials, electro-mechanical systems, and high-frequency components like
21 antennas). This technology has the potential to directly fabricate circuits on elastic and
22 bendable substrates as well as antennas on complementary metal-oxide-
23 semiconductor (CMOS) chips or on substrates with considerable topography. However, the
24 fabrication of 3D structures of high quality remains challenging. Here, a novel photosensitive
25 material is used for the additive fabrication of filigree three-dimensional (3D) conductive
26 silver microstructures of almost arbitrary geometry via LPR. The material is based on silver
27 perchlorate and gelatine solution. Structures fabricated with this material have a resistivity on
28 the order of $10^{-6} \Omega\text{m}$, a material density of approximately 95 %, and consist of almost 100
29 wt% silver. As a first functional component, a chiral metamaterial is presented.

30
31
32
33 Owing to the high demand for metallic microstructures, several techniques have been
34 developed for fabricating three-dimensional (3D) metallic microstructures.^[1-4] Usually, these
35 structures are fabricated via indirect methods. First, a template is manufactured using
36 subtractive micromachining or additive microfabrication. Thereafter, the metallic structure is
37 electrochemically grown inside the template, and the template is
38 removed subsequently.^[2] Although this method produces structures of outstanding quality, it
39 has two crucial disadvantages: limited freedom of design and difficulty with on-chip
40 fabrication. Considering this, it would be useful to have a direct method for fabricating
41 arbitrary microstructures on arbitrary substrates, such as circuits on elastic and bendable
42 substrates and antennas on CMOS chips or substrates. Further, this technique would be able to
43 produce microstructures with substantial topography. Most existing direct methods that enable
44 the fabrication of 3D metallic microstructures either require a conductive substrate (e.g.
45 electro-hydrodynamic printing) or have been slow thus far (e.g., electron beam-induced
46 deposition).^[4] Direct laser writing (DLW) via multiphoton absorption can quickly fabricate
47 almost arbitrary and highly accurate microstructures without the aforementioned drawbacks.
48 DLW uses a laser beam to selectively harden a photoresist via polymerisation.^[5-7] LPR,
49 similar to DLW, exploits multiphoton absorption but employs photo-reducing agents that
50 reduce the metal precursors. The fundamental building block of the microstructure is formed
51 via consequent nucleation, growth, and agglomeration (**Figure 1**).^[8-18] Some research groups

52 have exploited this mechanism to fabricate planar silver^[9-11] and gold^[12,13] as well as 3D
 53 silver^[14-16] and gold-composite microstructures^[17]. However, the full potential of this
 54 technology could not be exploited till now owing to the difficult-to-control chemical reactions
 55 involved with this method. While the quality of planar structures is similar to those of their
 56 polymeric counterparts, 3D metallic microstructures exhibited rather rough surfaces, had
 57 limited geometric complexity, and/or were formed from metal-polymer composite materials,
 58 which resulted in low conductivity.^[18] This is undesirable for high-frequency
 59 applications, because roughness leads to large scattering losses and large ohmic losses (in the
 60 case of composite materials). Therefore, for a novel photosensitive material, we focus on
 61 using liquid gelatine as a host matrix. It simultaneously functions as a reducing agent, viscous
 62 solvent for the silver precursor, and stabilising agent. Compared to a polymer matrix, it has the
 63 advantage of enabling and dispersing a large active substance load. Further, it is
 64 almost completely displaceable by the evolving silver structure and completely dissolvable
 65 under mild conditions. Overall, this material promises high purity and density and thus, high
 66 conductivity of the resulting microstructure, while preserving on-chip compatibility.
 67



68
 69 **Figure 1** (a) Laser-induced fabrication of metallic microstructures: A laser beam is focused by a high-numerical-aperture
 70 objective into a photosensitive material that is transparent at the wavelength of the laser used (780 nm). The power of the
 71 laser is adjusted via an acousto-optic modulator (AOM). Trajectories are scanned laterally using a galvanometer scanner
 72 or in three dimensions via a piezoelectric stage. (b) Fabrication process. Unexposed parts may be washed away. (c)
 73 Multiphoton absorption photoreduction, and subsequent nucleation, growth, and agglomeration steps take place to form the
 74 fundamental building block of the final structure.

75
 76 The strength of LPR is its versatility, in that it can fabricate almost every geometric shape. We
 77 demonstrate its versatility by fabricating numerous sample structures, with different
 78 geometries, using the novel material. The results are depicted in **Figure 2**; filigree helices,
 79 beams with right angles, but also structures with closed surfaces such as hollow pyramids, and
 80 an array of miniature horn antenna structures are observed. Overhanging structures are more
 81 challenging to fabricate compared to those fabricated along the downward writing direction
 82 (against the direction of laser beam propagation) because the radiation pressure drives
 83 evolving particles away from the structure rather than towards it. However, the right-angled
 84 beam in Figure 2(b) clearly demonstrates that such demanding structures are possible to
 85 fabricate by virtue of the high viscosity of gelatine. Naturally, upward writing directions are
 86 not possible with this approach because the pre-written structure parts block or attenuate the
 87 incoming laser radiation. However, similar to DLW, where structures are fabricated via a
 88 layer-by-layer top-down approach, fabricating structures in a top-down writing direction does
 89 not substantially limit the structural variety.
 90

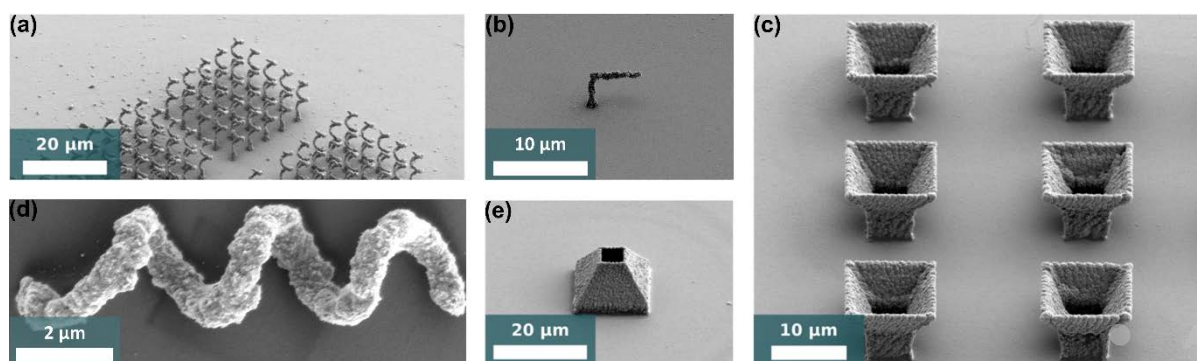


Figure 2 Diverse silver microstructures directly fabricated via laser-induced photoreduction. (a) Arrays of filigree helices. (b) A right-angled structure. (c) An array of miniature horn antennas. (d) A toppled helix. (e) A hollow pyramid.

91
92
93

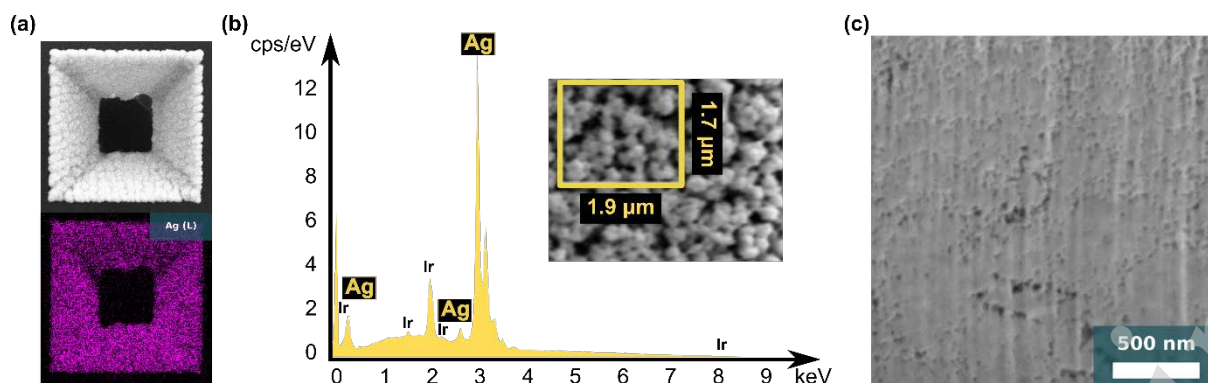
94
95

We determined the resolution, feature size, contour accuracy, and surface roughness of the structures presented in **Figure 2**. The smallest reproducible helix pitch is of 2 μm , and thus, the resist supports an axial resolution of 500 lines/mm. From the close-up of the helix (Figure 2(d)) that toppled during washing, we found that the lateral and axial feature sizes were nearly equal (approximately 760 nm). The spherical voxel possibly stemmed from the deteriorating effect of the evolving structure on the focal field. We measured the deviation of the diameter from the mean diameter of the helix as a measure for contour accuracy and found it to be in the order of ± 100 nm with a mean roughness of approximately ± 30 nm.

As shown in Figure 2 (c) and (e), closed structures with thin-walled silver surfaces may also be fabricated. However, since these structures were fabricated using a layer-by-layer writing approach and the laser-structure interaction played an important role in direct metal writing, these surfaces had some particularities to them. A wave-like topography with periodicity and an average pitch of approximately 670 nm was observed. This can be attributed to the same mechanism that is responsible for the formation of laser-induced periodic surface structures.^[16] The incident light interfered with scattered or diffracted light close to the surface of the structure. This additional topography reduced the contour accuracy compared to that of structures fabricated from a single line. Further, it led to a peak-to-valley deviation of the flat surface of approximately ± 150 nm.

As mentioned, gelatine enables the diffusion of the dissolved silver precursor and is displaced by growing silver seeds. Therefore, we expected structures with a high silver content and material density. **Figure 3**(a) shows an electron diffraction X-ray (EDX) count map and a corresponding scanning electron microscopy (SEM) analysis, which verified that silver is present only in the exposed parts. Furthermore, Figure 3(b) shows an EDX spectrograph acquired from the top of a freshly fabricated silver block (inset). An acceleration voltage of 10 kV was used for the measurement, and this corresponds to an approximate probing depth of 300 nm. Only silver and iridium (which appeared since we sputtered a 10 nm thick layer of it on top of the entire sample to avoid charging during SEM) was detected. This proves that the structures consist of almost 100 wt% silver close to their surface. EDX measurements of the internal parts (revealed by focused ion beam milling, not shown) of such blocks revealed approximately 99 wt% silver with some trace impurities (calcium, lead, and sulfur).

126

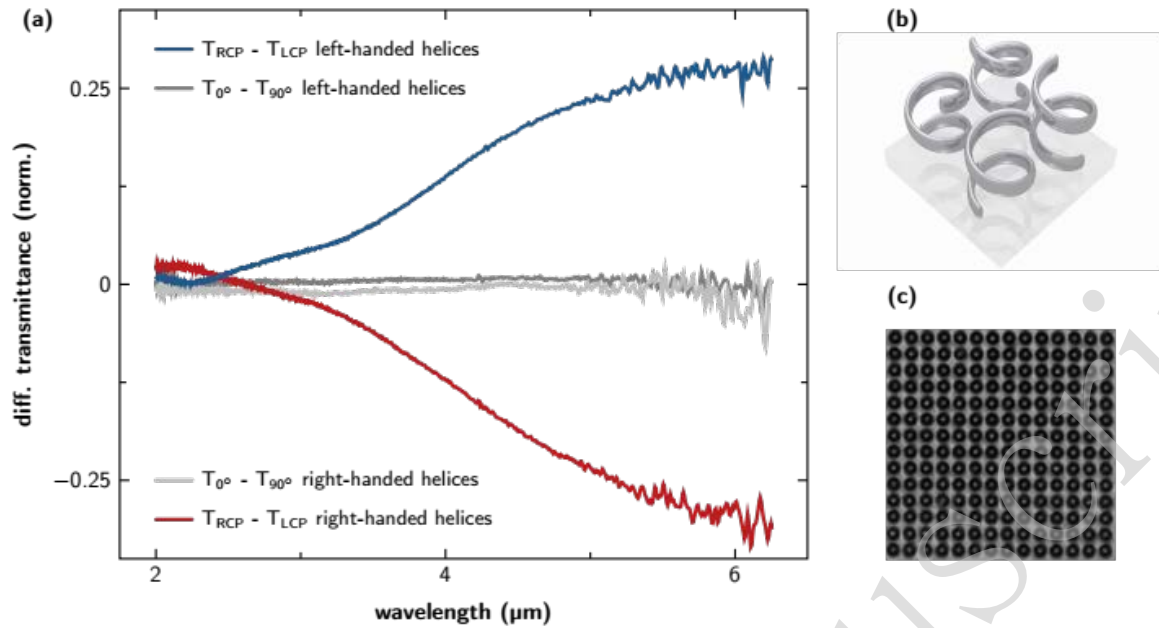


127
128 **Figure 3**(a) SEM images and EDX silver-count map of a 3D sample structure. (b) Electron diffraction X-ray spectrograph of
129 a freshly fabricated 3D sample structure verifying the high silver purity of the structure. Besides silver, only the peaks of
130 iridium are visible. The iridium peaks are due to post-fabrication sputtering of a 10 nm iridium layer that reduces charging
131 effects during SEM. The inset shows the region where the spectrum was acquired. (c) SEM image of a focused-ion-beam-
132 milled cross-section of a 3D sample structure showing a high material density and small average pore size.

133 From the milled cross-section, we also determined the material density and phase of the
134 internal microstructure of the fabricated structures (Figure 3(c)). The cross-section had an
135 average material density of 95% with an average pore diameter of 27 nm. The silver
136 structures were mostly composed of the amorphous phase, except in the vicinity of large voids.
137 The larger voids developed due to microexplosions occurring sporadically during writing up to
138 2 μm away from the substrate. Further away from the substrate, the writing process reached a
139 thermodynamic equilibrium that manifests in very stable writing conditions. Under those
140 conditions, the amorphous phase was favoured. Note that the fabrication power window is
141 exceedingly small (typically, a few tens of microwatts) because of the strong laser-matter
142 interaction. Thus, a small deviation from the optimal writing parameters decreases the material
143 density and surface roughness of the fabricated structures.

144 Since these structures exhibited high purity and material density, we also expected them to
145 show a high conductivity. Indeed, without annealing, the resistance of 3D wires (90 μm in
146 length and 1 μm in diameter) was measured to be on the order of 1.9 k Ω , which is almost three
147 orders of magnitude lower than the resistance of similar-sized gold-polymer
148 composite bridges.^[17] Further, the specific resistivity, calculated using a simple wire model, was
149 on the order of $3.3 \times 10^{-5} \Omega\text{m}$ (bulk silver: $1.6 \times 10^{-8} \Omega\text{m}$). It is well known that annealing
150 further reduces the resistivity. However, the high temperatures (several hundred degrees
151 Celsius) involved usually oppose on-chip compatibility of the material. Since gelatine melts at
152 moderate temperatures, we tested whether heating it at 50 $^{\circ}\text{C}$ has an influence on its resistivity.
153 Indeed, there was an exponential drop of resistivity over the heating time, and it approached
154 $6.7 \times 10^{-6} \Omega\text{m}$ after three hours. This value compared favourably with that of directly written
155 conductive polymers that, furthermore, only supported 2D structures.^[19] Thus, the material
156 enables the fabrication of conductive functional components. To prove this, we fabricated
157 arrays of helices in the C_4 geometry (Figure 4) with a diameter and pitch of 3 μm . Within the
158 unit cell, each of the helices had a phase shift of $\pi/2$ with respect to its direct neighbour to
159 avoid linear birefringence. The polarised Fourier transform infrared (FTIR) measurements on
160 a left- and right-handed set of helices demonstrated that only little linear birefringence was
161 observed (grey curves) (Figure 4(a)). Concurrently, these structures also had a strong
162 chiroptical response. While right-circularly polarised light was well transmitted over a broad
163 spectrum, the transmittance of left-circularly polarised light was strongly suppressed (blue
164 and red curves, respectively). The chiroptical responses clearly showed the expected mirror
165 symmetry, thereby demonstrating the high structural quality of the written arrays. Figure 4(b)
166 shows a rendering of the unit cell in C_4 symmetry. A light microscope image of a fabricated
167 array is depicted in Figure 4(c).

168



169
170 **Figure 4**(a) Linear (grey) and chiroptical response of left-handed (blue) as well as right-handed (red) helices fabricated in C_4
171 geometry. (b) Rendered image of the unit cell for a left-handed set of helices. (c) Transmission light micrograph of a typical
172 array of helices.

173
174

175 In summary, we have presented a novel photosensitive material that enables the fabrication of
176 filigree (highly conductive 3D silver microstructures) via laser-induced photoreduction. This
177 technique allows the fabrication of almost arbitrary 3D geometries, including right
178 angles. These structures have feature sizes below $1\ \mu\text{m}$ and a resistivity of approximately $10^{-5}\ \Omega\text{m}$
179 without annealing. Structures consisting of approximately 100 wt% silver have a
180 material density of approximately 95% and are mostly amorphous. This novel photosensitive
181 material paves the way for the direct on-chip fabrication of 3D functional electrical or optical
182 components. As a first application example, we demonstrate the chiroptical response of arrays
183 of helices.

184

185 Materials and Methods

186

187 *Preparation of photosensitive material:* A solution was prepared by heating 0.5 g of gelatine
188 (Roth Gold) in 10 mL of distilled water at $40\ ^\circ\text{C}$ for 3 h without stirring. The gelatine solution
189 was transparent at a writing wavelength of 780 nm, and it was used as a stock solution. To
190 this solution, 0.4 M AgClO_4 (Sigma Aldrich) was added and stirred at $40\ ^\circ\text{C}$ for 1 h (500 rpm)
191 using a magnetic stirrer. The photosensitive material was kept at room temperature (294
192 K) and remained in a liquid state.

193

194 *Fabrication process:* Glass plates (BK7, Schott) with a thickness and diameter of $170\ \mu\text{m}$ and
195 30 mm, respectively, were cleaned in an acetone ultrasonic bath for 10 min. This was
196 followed by a 10 min ultrasonic bath in isopropanol and subsequent rinsing using distilled
197 water. Two stripes of scotch tape were glued on the plate as spacers ($100\ \mu\text{m}$ height). The
198 photosensitive material was drop-casted on the plate between the spacers. A second glass
199 plate (18 mm square, BK7, Zeiss), cleaned in the same way, was placed on top of the spacers.
200 A home-built spatial-light-modulator-based DLW setup was used.^[20] The setup was built
201 around an 80 MHz pulsed femtosecond Ti:Sa laser (Chameleon Ultra VIS, Coherent) operated

202 at a wavelength of 780 nm and an inverted microscope (Axio Observer, Zeiss). To
203 ensure compatibility of the presented photosensitive material with commercially available
204 DLW systems, we did not change the wavelength. The power of the laser was controlled using
205 an acousto-optical modulator (3080-125, Crystal Technology), and the aberration correction
206 was enabled by a spatial-light-modulator (X10468-02, Hamamatsu). The laser was focused
207 into the resist using a high-numerical-aperture objective lens (NA=1.4, 63x, Leica). The
208 filigree structures were fabricated by slowly moving the sample with piezo-electrical stages at
209 speeds of approximately 1 $\mu\text{m/s}$, while compact structures required speeds up to 20 $\mu\text{m/s}$.
210 Typically, a few milliwatts of laser power were required for the fabrication.

211
212 *Post-process:* To remove unexposed parts, a small drop of the photosensitive material was
213 casted on the sample. Subsequently, the sample was rinsed with distilled water and gently
214 blow-dried using nitrogen gas.

215
216 *Resistivity measurements:* Two silver electrodes, separated by approximately 90 μm , were
217 prepared via sputtering and cutting using a razor blade. We verified that the electrodes were
218 not electrically connected using a linear four-point measurement setup. Subsequently, the
219 novel silver resist was used to fabricate a 10 μm -high silver bridge across the gap. The bridge
220 had a diameter of approximately 1 μm . After washing and blow drying, the four-point
221 measurement setup was used to determine the resistance of the 3D structure from the fitted
222 slope of I - V curves. To determine the resistivity, the above geometric dimensions and a
223 simple wire model were used:

$$\rho = \frac{R \cdot A}{L}$$

224
225
226 where R is the measured resistance, L is the length of the wire, and A is its cross-sectional area.
227
228

229 *FTIR measurements:* FTIR measurements of the helices were conducted using a Bruker Vertex
230 80 FTIR spectrometer coupled to a Bruker Hyperion 2000 microscope. To generate circular-
231 polarised light, a combination of an infrared linear polariser (Thorlabs WP25H) and a super
232 achromatic quarter-waveplate (B. Halle Nachf., customised) was used. The arrays of the
233 helices used for the measurements had a footprint of 150 \times 150 μm^2 . The measured area was
234 set to 120 \times 120 μm^2 , and the spectra were normalised with respect to the substrate.

235 236 **Acknowledgements**

237 Funded by the Deutsche Forschungsgemeinschaft (DFG, German Research Foundation) –
238 Project-ID 172116086 – SFB 926. Fraunhofer Cluster of Excellence Advanced Photon
239 Sources (CAPS). We are grateful for the support of the Nano Structuring Center (NSC) at the
240 Technische Universität Kaiserslautern.

241 242 243 **Conflict of interests**

244 The authors declare no conflict of interests.

245 246 **Contributions**

247 E.H.W. developed the materials, fabricated the structures, and characterised the samples. J. K.
248 performed the FTIR measurements. E.H.W and G.v.F. designed the experiments. All authors
249 discussed the results and wrote the paper.

250 251 **References**

- 252 1 Avayu, O. *et al.* Composite functional metasurfaces for multispectral achromatic
253 optics. *Nature Communications* **8**, 14992 (2017).
- 254 2 Gansel, J. K. *et al.* Gold helix photonic metamaterial as broadband circular
255 polarizer. *Science* **325**, 1513-1515 (2009).
- 256 3 Stärke, P. *et al.* High-efficiency wideband 3-D on-chip antennas for subterahertz
257 applications demonstrated at 200 GHz. *IEEE Transactions on Terahertz Science*
258 *and Technology* **7**, 415-423 (2017).
- 259 4 Hirt, L. *et al.* Additive manufacturing of metal structures at the micrometer
260 scale. *Advanced Materials* **29**, 1604211 (2017).
- 261 5 Hahn, V. *et al.* Rapid assembly of small materials building blocks (Voxels) into
262 large functional 3D metamaterials. *Advanced Functional Materials* **30**, 1907795
263 (2020).
- 264 6 Maruo, S., Nakamura, O. & Kawata, S. Three-dimensional microfabrication with
265 two-photon-absorbed photopolymerization. *Optics Letters* **22**, 132-134 (1997).
- 266 7 Hohmann, J. K. *et al.* Three-dimensional μ -printing: an enabling
267 technology. *Advanced Optical Materials* **3**, 1488-1507 (2015).
- 268 8 Waller, E. H. & von Freymann, G. From photoinduced electron transfer to 3D
269 metal microstructures via direct laser writing. *Nanophotonics* **7**, 1259-1277 (2018).
- 270 9 He, G. C. *et al.* The conductive silver nanowires fabricated by two-beam laser
271 direct writing on the flexible sheet. *Scientific Reports* **7**, 41757 (2017).
- 272 10 Xu, B. B. *et al.* Flexible nanowiring of metal on nonplanar substrates by
273 femtosecond-laser-induced electroless plating. *Small* **6**, 1762-1766 (2010).
- 274 11 Tabrizi, S. *et al.* Functional optical plasmonic resonators fabricated via highly
275 photosensitive direct laser reduction. *Advanced Optical Materials* **4**, 529-533
276 (2016).

- 277 12 Lee, M. R. *et al.* Direct metal writing and precise positioning of gold nanoparticles
278 within microfluidic channels for SERS sensing of gaseous analytes. *ACS Applied*
279 *Materials & Interfaces***9**, 39584-39593 (2017).
- 280 13 Lu, W. E. *et al.* Femtosecond direct laser writing of gold nanostructures by ionic
281 liquid assisted multiphoton photoreduction. *Optical Materials Express***3**, 1660-
282 1673 (2013).
- 283 14 Tanaka, T., Ishikawa, A. & Kawata, S. Two-photon-induced reduction of metal
284 ions for fabricating three-dimensional electrically conductive metallic
285 microstructure. *Applied Physics Letters* **88**, 081107 (2006).
- 286 15 Liu, L. P. *et al.* Fast fabrication of silver helical metamaterial with single-exposure
287 femtosecond laser photoreduction. *Nanophotonics***8**, 1087-1093 (2019).
- 288 16 Barton, P. *et al.* Fabrication of silver nanostructures using femtosecond laser-
289 induced photoreduction. *Nanotechnology***28**, 505302 (2017).
- 290 17 Blasco, E. *et al.* Fabrication of conductive 3D gold-containing microstructures via
291 direct laser writing. *Advanced Materials* **28**, 3592-3595 (2016).
- 292 18 Waller, E. H. *et al.* Functional metallic microcomponents via liquid-phase
293 multiphoton direct laser writing: a review. *Micromachines***10**, 827 (2019).
- 294 19 Luo, Z. J. *et al.* Direct laser writing of nanoscale undoped conductive
295 polymer. *Nanotechnology***31**, 255301 (2020).
- 296 20 Waller, E. H., Renner, M. & von Freymann, G. Active aberration- and point-
297 spread-function control in direct laser writing. *Optics Express* **20**, 24949-24956
298 (2012).